

1 **Source time function clustering reveals patterns in**
2 **earthquake dynamics**

3 **Jiuxun Yin¹, Zefeng Li², Marine Denolle¹**

4 ¹Department of Earth and Planetary Sciences, Harvard University, Cambridge, MA, USA

5 ²Seismological Laboratory, Division of Geological and Planetary Sciences, California Institute of
6 Technology, Pasadena, CA, USA

7 **Key Points:**

- 8 • We cluster earthquakes based on the dynamic time warping distance of their source
9 time function (STF) shapes.
10 • The patterns of complexity correlate with source parameters such as depth, mech-
11 anism, and radiation.
12 • Simulations of dynamic rupture indicate a correlation between the STF complex-
13 ity and frictional properties.

Corresponding author: Zefeng Li, zefengli@caltech.edu

14 **Abstract**

15 In this study, we cluster a large number of earthquake source time functions (STFs) and
 16 explore the relations between the clusters and earthquake properties. We use the dynamic
 17 time warping (DTW) distance and hierarchical clustering to group earthquakes based
 18 on the general shape of their STFs. We apply this to a global data base of 3529 STFs
 19 from earthquakes of magnitude greater than M_W 5.5 between 1995 and 2018. The clus-
 20 ters exhibit different degrees of STF shape complexity, as measured by the number of
 21 prominent peaks. The clustering also indicates an association between the degree of STF
 22 complexity (or group) and earthquake source parameters. Thrust mechanism are in large
 23 proportion events with simple STF shapes and at all depths. In contrast, complex STF
 24 shapes correspond to shallow earthquakes with larger proportion of strike-slip mecha-
 25 nism and a generally longer duration. Moreover, we find that earthquakes with complex
 26 STF shapes tend to locate in the regions with complicated tectonics. These findings are
 27 corroborated by 2D dynamic modeling of earthquake ruptures on heterogeneous pre-stress
 28 and linear slip-weakening friction. We find a systematic variation of the simulated STF
 29 complexity with frictional properties. The clustering distribution provides useful con-
 30 straints on elements of the frictional properties. In particular, the characteristic slip-weakening
 31 distance could be constrained to be over all short (< 0.1 m) and depth dependent.

32 **Plain Language Summary**

33 Seismic waves carry a signature about the earthquake source process. Earthquake
 34 source time functions (STFs), which are directly recovered from seismic waves, reflect
 35 the temporal history of earthquake rupture. However, it is often hard to directly com-
 36 pare STFs due to the large differences among earthquakes in terms of amplitude and du-
 37 ration. In this study, we perform a cluster analysis of STFs using a technique called dy-
 38 namic time warping (DTW). DTW is commonly used in speech recognition to handle
 39 with various speeds of elocution. DTW allows us to dynamically stretch the seismic sig-
 40 nals and provides a new way to quantify earthquake similarity through analyzing the shapes
 41 of their source time functions (STFs). We apply this to a large database of STFs. Our
 42 results show that the shape complexity of STFs is correlated with the earthquake source
 43 parameters such as the earthquake depth, focal mechanism, and energy radiation. Our
 44 numerical simulations further show that those correlations may indicate a spatial het-
 45 erogeneity of frictional properties.

46 **1 Introduction**

47 Earthquakes are known to break in diverse manners: some events rupture on a ge-
 48 ometrically simple fault with a relatively smooth slip distribution (e.g., Yagi & Fukahata,
 49 2011), while others break a network of faults and/or have heterogeneous slip distribu-
 50 tion (Li et al., 1994; Ammon et al., 2005; Meng et al., 2012; Cesca et al., 2017). Although
 51 the complexity of earthquakes can be directly observed, in some cases, from surface fault
 52 trace (Massonnet et al., 1993; Li et al., 1994; Kaneko et al., 2017), many ruptures are
 53 buried at depth so that seismic waves are the only observations available to infer the source
 54 process. Derived from seismic waves through waveform deconvolution or kinematic in-
 55 version, the earthquake Source Time Function (STF) is a foremost important seismic ob-
 56 servation that describes the time history of moment release during a rupture. Moreover,
 57 the shape of the STF directly controls the variability and uncertainty in the strength and
 58 duration of strong ground motion.

59 Observations of global earthquake STFs and source spectra have shown significant
 60 inter-event variability among earthquakes (Allmann & Shearer, 2009; Atik et al., 2010;
 61 Denolle, 2019). Such variability may partly come from differences in data processing strat-
 62 egy (Ide & Beroza, 2001). Therefore, large catalogs of STFs (or their spectra) obtained
 63 from a uniform approach is preferable to analyze relative differences among earthquakes

(Allmann & Shearer, 2009; Convers & Newman, 2011; Denolle & Shearer, 2016; Vallée & Douet, 2016).

Recently, such catalogs of STF (or of their spectra) have enabled multiple discoveries about earthquake source processes. For example, the total seismic moment M_0 (the time integral of the STF) scales with source duration T^3 (the duration of the STF) for most small to moderate size earthquakes, which implies that the earthquake stress drop is roughly invariant with earthquake magnitudes. At larger magnitudes, this scaling may differ (e.g. $M_0 \sim T^2$ from Denolle and Shearer (2016)). Their properties also have indicated that the ratio of the radiated energy E_R over the moment, also referred to as the scaled energy E_R/M_0 , varies spatially and with depth but remains invariant with earthquake magnitude (Convers & Newman, 2011; Baltay et al., 2014; Denolle & Shearer, 2016).

However, both the amplitude and the source duration of the STF vary by orders of magnitude. This requires careful strategies of amplitude and time scaling for across-magnitude visualization and comparison. One approach is to scale the time axis to a duration metric and normalize the amplitude to seismic moment (i.e. the integral of the STF). However, source duration is difficult to measure because near-source and near-site scattering of seismic waves may interfere with waves radiating from the end of the seismic rupture. Therefore previous studies have proposed several metrics of duration: moment-based duration (Houston, 2001), threshold-based duration (Vallée, 2013; Denolle, 2019), and centroid-based duration (Meier et al., 2017). Because these measures are not strictly equivalent, the shapes of the scaled and stretched STFs differ as well. For instance, Meier et al. (2017) find that average STFs have rather a triangle shape whereas Denolle (2019) suggests a rather skewed-Gaussian functional form.

Here, we propose to weaken the assumption of a particular definition of source duration and instead use dynamic time warping (DTW) to compare the shapes of the STFs. DTW has been widely used in speech recognition (Berndt & Clifford, 1994; “Dynamic Time Warping”, 2007). The DTW algorithm performs a non-uniform stretching of time and amplitude to match the shape of two time series via the optimal warping path with minimum distance (Figure S1). We measure the similarity between STFs with DTW distance and cluster the STFs accordingly. We apply this to the global SCARDEC catalog of STFs (Vallée & Douet, 2016, available at <http://scardec.projects.sismo.ipgg.fr/>, last accessed 01/20/2020) that contains 3529 earthquakes of magnitude greater than 5.5 from 1/1/1992 and until 12/31/2018. The analysis shows that the STF overall shape is correlated with several earthquake source parameters, such as focal mechanisms, depth, and scaled energy.

To test whether the current physical understanding of earthquake processes reproduces the clustering patterns, we perform dynamic simulations of earthquake ruptures with linear slip-weakening friction to construct synthetic STFs. We find a strong correlation between the grouping distribution of STF shapes and frictional parameters, such as the characteristic slip-weakening distance D_c . Furthermore, we find that the grouping pattern of the SCARDEC STF shapes are most similar to those simulated STFs with small values of D_c , thus the grouping patterns of a large number of STFs can potentially provide observational constraints to earthquake dynamics.

2 Dynamic time warping and clustering analysis

DTW measures the similarity between two time series that may not share the same frequency content or the same sampling rate. The series are “warped” (or stretched) non-uniformly in the time dimensions to optimally match two series (Figure S1). This algorithm is widely used in automated speech recognition in which different audio sequences may have different speaking speeds (Berndt & Clifford, 1994; “Dynamic Time Warping”, 2007). One important advantage of DTW is its ability to preserve topological structures

114 of the time series by assimilating their temporal elongation or compression. Once stretched,
 115 the DTW distance is taken as a new metric for STF similarity, which can be used for
 116 clustering. Our approach follows four steps: 1) STF pre-conditioning, 2) DTW distance
 117 calculation, 3) clustering, 4) re-grouping around a centroid event.

118 We first perform minimal pre-conditioning of the STF shapes. The STFs are built
 119 from the deconvolution of teleseismic P waves that are relatively well constrained at fre-
 120 quencies below 1 Hz (Vallée & Douet, 2016). Given that the maximum duration of the
 121 STF in the catalog is about 100 s, we re-sample the data to 100 points giving a mini-
 122 mum sampling rate of 1 point per second. We then normalize the amplitude STFs to the
 123 event seismic moment. These two processing steps improve the stability of the warping.
 124 We have tested various strategies to resample and normalize the STFs, which did not
 125 affect the conclusions of this analysis.

126 Second, we apply the DTW to each pair of STFs. The DTW distance is the Eu-
 127 clidean distance between two STFs warped along the optimal warping path, and is cho-
 128 sen here as the measure of similarity between two STFs (see Figure S1 (a)-(b)).

129 Then, the STF shapes are clustered based on their DTW distance with a single-
 130 linkage hierarchical clustering analysis that provides the flexibility to form clusters at
 131 any desired level (Text S1, Figure S1 (c)). Here, we constrain the number of clusters to
 132 be 20, which is about equivalent of DTW distance threshold of 0.4. For each of these clus-
 133 ters, we choose a representative STF (defined as the centroid event) that has the mini-
 134 mum median distance with all of the other members of the cluster. It is similar to the
 135 stack of all stretched STF within each cluster (Figure 1), which, in turn, exhibits the com-
 136 mon features of all cluster members.

137 Furthermore, we parameterize the characteristic STF shape for each of these clus-
 138 ters by calculating the number of prominent peaks of each centroid event. The number
 139 of prominent peaks is commonly used for topographic relief analysis and is defined as
 140 the amplitude of the peak (hill summit) relative to the lowest amplitude point (valley)
 141 that does not contain a higher peak. This metric differs from the calculation of Gaus-
 142 sian subevents that Danré et al. (2019) use. One hyper-parameter we tune is a thresh-
 143 old for peak amplitude of the prominent peak, which we choose to be 10% of the global
 144 maximum of the STF amplitude. The raw and stretched STFs have a lot fewer promi-
 145 nent peaks than individual peaks from the Gaussian decomposition by Danré et al. (2019)
 146 (Figure S2). Furthermore, the stretched STFs have fewer prominent peaks than the raw
 147 STFs, but in general the same number of prominent peaks as the centroid event (Fig-
 148 ure S3). For instance, a STF may have multiple separated amplitude peaks, but only one
 149 single prominent peak (Figure 1 (a)-(b)).

150 Finally, we group the clusters based on the number of prominent peaks of the cen-
 151 troid event, where G1 is the group where the centroid event has 1 prominent peak, G2
 152 is the group where the centroid event has 2 prominent peaks, ... (Figure 1 (c)). G4 is
 153 the group where the centroid event has at least 4 prominent peaks. Examples of detected
 154 prominent peaks are found in Figure 1 (a)-(b) (see Figure S4 for the unstretched STFs).
 155 In this study, we define the STFs to be “complex” if their DTW stretched STFs have
 156 multiple prominent peak. The first order result from the grouping is that most events
 157 have a single prominent peak whereas about 20% events are more complex.

158 **3 Correlations between shape complexity and source parameters**

159 We now explore the correlation between grouping and several source parameters
 160 such as depth, focal mechanism, moment, duration, energy, and location.

161 The first property we investigate is the source depth. Complex STFs (groups G2-
 162 G4) are mostly shallow crustal events (≤ 20 km) whereas the simple STFs (group G1)

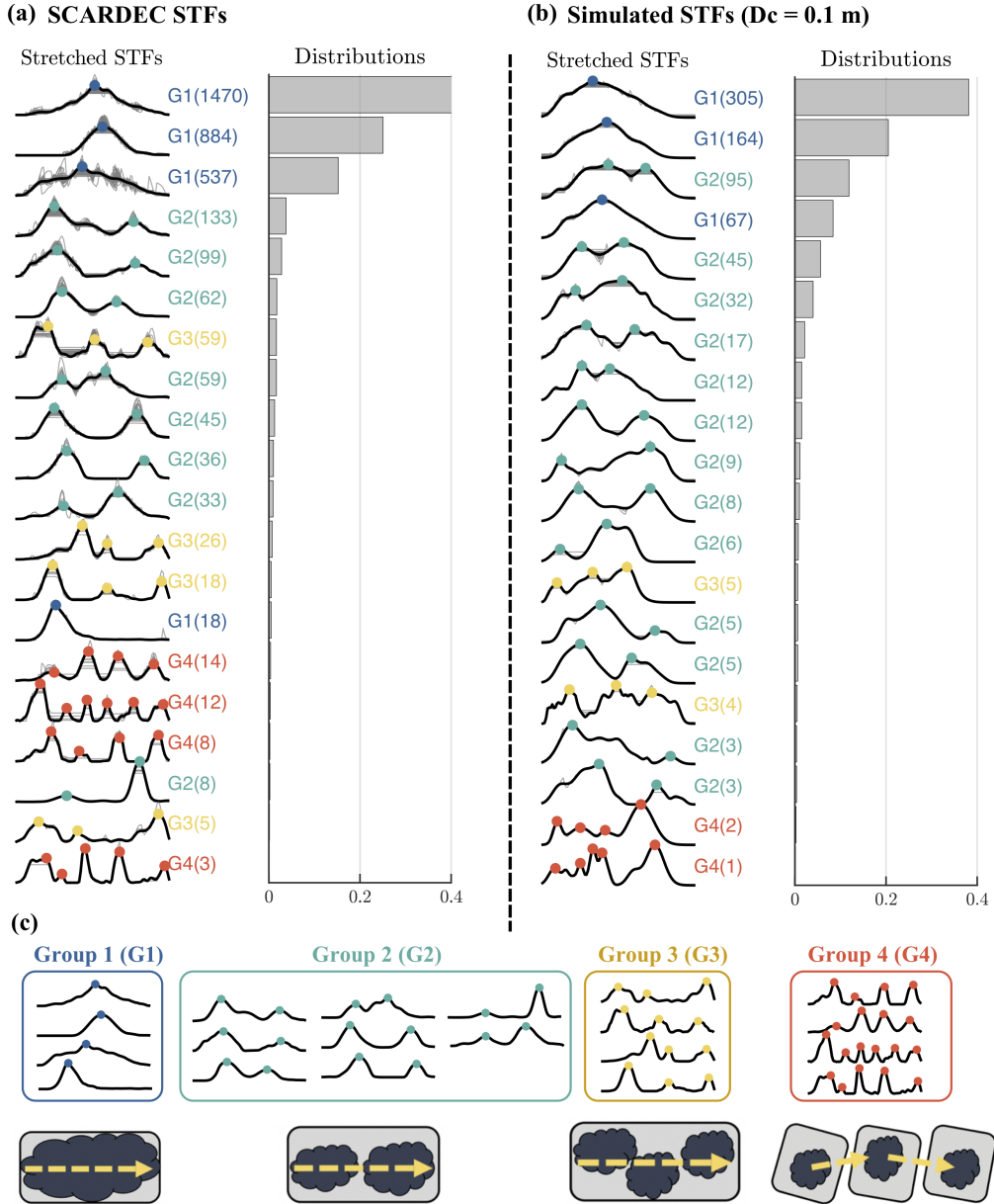


Figure 1. Source time function clustering, grouping, and conceptual interpretation. (a) Individual STFs after dynamic time warping and clustering are shown by gray thin lines. Black thick lines are the STFs of the centroid event of each cluster. Colored dots indicate the prominent peaks of the centroid STF as well as the associated group. Numbers in the parentheses are the number of STFs in each cluster. The corresponding population proportion of each cluster is shown in the right histograms. (b) Same as (a) but for the STFs from our dynamic simulations. (c) Cluster centroid STF shapes and conceptual models for G1-G4. In the model diagram, dark blocks represent major rupture asperities and the arrow indicates the rupture direction.

163 can be found at all depths (Figure 2 (a)). Because co-located events have various degrees
 164 of complexity (Figure 2 (d), Figure 3), inaccuracy in the Green's function does not strongly
 165 bias these specific results.

166 The second property we investigate is the focal mechanism (Figure 2 (b)). The fo-
 167 cal mechanisms are solved simultaneously by the SCARDEC method (Vallée et al., 2011).
 168 Most of the thrust earthquakes have simple STF's (G1 and G2), whereas the strike-slip
 169 earthquakes are dominated by complex STF's (G3 and G4). There are too few normal
 170 events in the database (only 17.5 %) to give any significant conclusion regarding this
 171 mechanism.

172 There is no clear relation between earthquake size (moment) and this metric of com-
 173 plexity (see Figure 2 (d) and Figure S5). For example in Figure 2 (d), we see that the
 174 largest events in SCARDEC database may only have one prominent peak in their stretched
 175 STF, while the events with smaller moments can be in any of those complexity groups.

176 We find a clear pattern that G3-G4 events have an abnormally longer duration with
 177 respect to other events of similar magnitudes and relative to events of the other groups
 178 (Figure 2 (d)). It is illustrated in Figure 2 (d) by visualization of two STF's of co-located
 179 events and of similar magnitudes. For the same earthquake moment (or the STF inte-
 180 gral), it is intuitive to understand that STF's in G4 have multiple low amplitude promi-
 181 nent peaks and overall extended duration, compared to the G1 STF's that have a sin-
 182 gle high amplitude and short duration peak. Simple models of crack ruptures yield a re-
 183 lation between moment, source duration, and stress drop that could indicate low stress
 184 drops for the G4 events (Figure S6 (a)-(c)) (Brune, 1971; Eshelby, 1957).

185 We now explore the clustering results against the earthquake scaled energy. Here
 186 we calculate radiated energy from the squared time derivative of the STF (moment ac-
 187 celeration function $\ddot{M}_0(t)$) using the relation $E_R = (\frac{1}{15\pi\rho V_p^5} + \frac{1}{10\pi\rho V_s^5}) \int_0^\infty (\ddot{M}_0(t))^2 dt$.
 188 We select depth-dependent bulk properties (V_p , V_s , ρ) from PREM (Dziewonski & An-
 189 derson, 1981). Radiated energy scales almost linearly with seismic moment and look at
 190 the scaled energy, the ratio of both radiated energy and seismic moment. Figure 2 (c)
 191 shows the distribution of the scaled energy with respect to each group. G3 and G4 events
 192 have systematically larger scaled energy as G1 and G2 events. This is consistent with
 193 intuition that G3 and G4 events generally have rougher STF's.

194 The correlations between STF complexity and source depths and focal mechanism
 195 are consistent with the findings from previous studies (Houston, 2001; Vallée, 2013; Danré
 196 et al., 2019). In particular, shallow strike slip earthquakes are constrained geometrically
 197 by the Earth surface on the top and the seismogenic depth on the bottom. They also
 198 tend to be composed of segmented faults (Klinger, 2010). These geometrical settings con-
 199 trol the evolution of rupture that tends to operate with moving energetic slip pulses (Kaneko
 200 & Lapusta, 2010) with repeated rupture acceleration and deceleration as they travel across
 201 segments (e.g., Kanamori et al., 1992; Peyrat et al., 2001; Cesca et al., 2017).

202 Since earthquake source parameters are closely related to the local tectonic regime,
 203 we also find that our observations from the clustering and grouping results (G1 - G4)
 204 are consistent to the marked variation of tectonic environments (Figure 3). Many of the
 205 major subduction zones are dominated by the simpler types of events (G1 and G2) and
 206 lack of more complex ones, likely because they are dominated by thrust events located
 207 along/within the subducting slabs at various depths. For example, since 1992, there have
 208 been only two events ($M_W > 5.5$) belonging to the G3 group along the Southern Amer-
 209 ican and Aleutian subduction zones, respectively (Figure 4 (a)-(b)). Similarly, other sub-
 210 duction zone regions like in Japan and in Sumatra, the Indian-Eurasian collision zone
 211 are also dominated by simple-type earthquakes (Figure 4 (c)-(d)). In contrast, the com-
 212 plex group (G3 and G4) events are located mostly along the boundaries around the junc-
 213 tion region of the Indo-Australian, western Pacific, Philippine plates and Eurasian plates
 214 (Figure 3 and Figure 4 (e)). Bird (2003) explored and documented the kinematics at plate
 215 boundaries and found that this region is characterized by a particularly extensive num-
 216 ber of micro plates, whose boundaries exhibit varied relative motions and kinematics (their

217 Figure 6). Therefore, we propose that the complexity in the STF may reflect the com-
 218 plexity in the regional stress field.

219 4 Modeling STF complexity

220 Simulations of dynamic ruptures using stochastic distributions of fault-interface pa-
 221 rameters are popular in the investigations of complex kinematic source models, realis-
 222 tic fault geometry and roughness models, and to simulate high-frequency ground motions
 223 (Mai & Beroza, 2002; Ripperger et al., 2007; Trugman & Dunham, 2014; Graves & Pitarka,
 224 2016; Mai et al., 2017). In order to investigate possible factors that control the STF com-
 225 plexity patterns, we perform a large number of 2-dimensional dynamic rupture simula-
 226 tions with stochastic distributions of pre-stress, and apply the same clustering analysis
 227 to the resulting synthetic STFs as to the SCARDEC STFs.

228 In this study, synthetic dynamic sources are generated in a 2-dimensional medium
 229 in an anti-plane setting. Pre-stress on the fault is constrained to follow a power-law am-
 230 plitude distribution that approximates the scenario caused by natural fault roughness
 231 (Candela et al., 2012, Text S2 for more details). We assume a constant normal stress of
 232 120 MPa and linear slip weakening friction law (Andrews, 1976). Linear slip weakening
 233 requires three parameters: the static friction coefficient (here chosen as $\mu_s = 0.677$),
 234 the dynamic friction coefficient (here chosen as $\mu_d = 0.525$), and the characteristic slip-
 235 weakening distance D_c . We set up the experiments so that the fault-average stress drop
 236 is about 1 MPa (Figure S7).

237 Danré et al. (2019) find that heterogeneity is necessary to reproduce realistically
 238 rough STFs. Here, we focus on varying D_c , yet aware of the trade-off between strength
 239 excess and D_c in controlling rupture velocity and the resulting ground motions (Guatterri
 240 & Spudich, 2000). While we keep D_c constant within a single set of simulations, we carry
 241 several sets of experiments with values of D_c at various levels 0.05, 0.1, 0.2, 0.4, 0.8, and
 242 1.6 m that are within bounds found in the literature.

243 For each D_c , we first generate a set of pre-stress distributions that we use in each
 244 simulations. The dynamic rupture is solved by 2D boundary integral method SBIEM-
 245 LAB (<http://web.gps.caltech.edu/~ampuero/software.html>, last accessed 11/27/2018).
 246 We discard the rupture models that unsuccessfully nucleated with a source dimension
 247 less than 20 km, or rupture beyond the zone of heterogeneous pre-stress, and obtain 800
 248 qualified simulations for each D_c value. Finally, the STFs are calculated from the inte-
 249 gral of the moment-density-rate functions over the fault surface (more details in Text
 250 S2).

251 We perform the hierarchical clustering and group the simulated STFs for each D_c ,
 252 following the same procedures as for the SCARDEC STFs (Figure 1 (b), Figures S8 -
 253 S12). Because our modeling is not three dimensional and does not include the free sur-
 254 face, we are not matching observations such as the focal mechanism and depth. How-
 255 ever, our results can match the proportion of the STFs relative to each group: 80% of
 256 the STFs belong to the G1 group, 15% belong to the G2, and the rest in higher indexed
 257 groups. Comparison of the relative proportion between groups for each set of simulations
 258 suggests that an increasing D_c value yield an increase in STF complexity (e.g. propor-
 259 tion of G3-G4 events). This shows that D_c , or more generally, the frictional parameters
 260 can impact the complexity of STFs. Compared with the observed global variability in
 261 SCARDEC STFs, small value of D_c (< 0.1 m) is preferred in this particular metric of
 262 complexity. In contrast, models with large value of D_c tend to generate proportionally
 263 more STFs belonging to G3 beyond (Figures S10 - S12).

264 Our results indicate that the small values of $D_c < 0.1$ m are necessary to produce
 265 the general level of complexity of the SCARDEC STFs (Figure 5 (a)). When binning
 266 these relative contributions with source depths, we find that crustal events ($h \leq 40$ km),

267 which show a higher degree of complexity, could be explained by a larger D_c value than
 268 the deeper events (Figure 2 (a), Figure 5 (b)). This is more pronounced with the upper-
 269 crustal depths ($h \leq 20$ km).

270 Depth variations in D_c have been reported in earlier studies. Wibberley and Shi-
 271 mamoto (2005) perform laboratory experiments on samples from the Median Tectonic
 272 Line in southwestern Japan, and estimate that D_c ought to vary with depth, with a deeper
 273 (6 km) values being systematically 30% smaller than the shallow (2 km) values. Kine-
 274 matic source inversions also find a systematic depth variation of rise time, which they
 275 attribute to a systematic dependence in D_c (Ide & Takeo, 1997). Our results may pro-
 276 vide a supporting evidence that the characteristic slip-weakening distance varies at depth
 277 over crustal scales.

278 5 Discussion and Conclusion

279 We apply a dynamic time warping methodology to cluster a large number of earth-
 280 quake source time functions based on similarity of their general shapes. We find patterns
 281 between source parameters and the STF shape, which we now compare with previous
 282 work Danré et al. (2019) that analyzed the same SCARDEC database. Although the def-
 283 inition of complexity in Danré et al. (2019) is different, this study confirms the corre-
 284 lation between STF complexity with focal depth and mechanisms. This study adds to
 285 the Danré et al. (2019) in three ways. First, there is no correlation between this partic-
 286 ular metric of complexity and earthquake magnitude. This means that the shape of the
 287 individual prominent peaks does not systematically change with earthquake magnitude,
 288 while the number of individual and separated peaks does. Second, we analyze in this study
 289 the relation between degree of complexity and other source parameters, such as the scal-
 290 ing between duration and moment (sometimes used to estimate earthquake stress drop)
 291 and the ratio between radiated energy and moment. Taken together, it is reasonable to
 292 infer that the complex STFs exhibit large radiation ratio (proportion of radiated energy
 293 over available energy).

294 Finally, the modeled STFs exhibit different degrees of complexity depending on the
 295 frictional properties. We find that small values of characteristic slip weakening distance
 296 are required to reproduce the variability in complexity measured in the SCARDEC database.
 297 Furthermore, we find that the variability in STF complexity of shallow earthquakes is
 298 better explained by a larger value of characteristic distance compared to the deeper sources.

299 There are several limitations to our approaches. First, the database we use is con-
 300 structed from a Green's function in a radially symmetric Earth. Although this is unlikely
 301 to affect the overall results, Green's functions that account for laterally varying struc-
 302 ture would improve the temporal resolution of the shallowest events. This requires bet-
 303 ter understanding of near surface scattering and attenuation. Second, our modeling ap-
 304 proach is unable to characterize the correlation between focal mechanisms and STF com-
 305 plexity. Indeed, these parameters could be tested using a 3-dimensional dynamic rup-
 306 ture simulation framework, which however is impractical to implement due to high com-
 307 putational expense and the employed statistical approaches. Nevertheless, because fault
 308 geometry and fault properties seem to play a dominant role in shaping the source and
 309 the resulting strong ground motions, further 3-dimensional modeling and observations
 310 are necessary.

311 Acknowledgments

312 We sincerely thank Martin Vallée for his insightful suggestions. All the source time func-
 313 tions are downloaded from SCARDEC source time function database (<http://scardec.projects.sismo.ipgp.fr/>). The dynamic rupture simulation code SBIEMLAB is de-
 314 veloped by Jean-Paul Ampuero (available on <http://web.gps.caltech.edu/~ampuero/>)
 315

316 `software.html`). The Matlab scripts to reproduce the results and figures can be obtained
 317 on the Github (https://github.com/yinjiuxun/STF_DTW). Global maps are made by
 318 GMT (Wessel et al., 2013, available at <http://gmt.soest.hawaii.edu/>).

319 References

- 320 Allmann, B. P., & Shearer, P. M. (2009). Global variations of stress drop for mod-
 321 erate to large earthquakes. *Journal of Geophysical Research: Solid Earth*,
 322 *114*(B1), B01310. doi: 10.1029/2008JB005821
- 323 Ammon, C. J., Ji, C., Thio, H.-K., Robinson, D., Ni, S., Hjorleifsdottir, V., ...
 324 Wald, D. (2005). Rupture Process of the 2004 Sumatra-Andaman Earthquake.
 325 *Science*, *308*(5725), 1133–1139. doi: 10.1126/science.1112260
- 326 Andrews, D. J. (1976). Rupture propagation with finite stress in antiplane
 327 strain. *Journal of Geophysical Research*, *81*(20), 3575–3582. doi: 10.1029/
 328 JB081i020p03575
- 329 Atik, L. A., Abrahamson, N., Bommer, J. J., Scherbaum, F., Cotton, F., & Kuehn,
 330 N. (2010). The Variability of Ground-Motion Prediction Models and
 331 Its Components. *Seismological Research Letters*, *81*(5), 794–801. doi:
 332 10.1785/gssrl.81.5.794
- 333 Baltay, A. S., Beroza, G. C., & Ide, S. (2014). Radiated Energy of Great Earth-
 334 quakes from Teleseismic Empirical Green’s Function Deconvolution. *Pure and*
 335 *Applied Geophysics*, *171*(10), 2841–2862. doi: 10.1007/s00024-014-0804-0
- 336 Berndt, D. J., & Clifford, J. (1994). Using dynamic time warping to find patterns in
 337 time series. In *KDD workshop* (Vol. 10, pp. 359–370). Seattle, WA.
- 338 Bird, P. (2003). An updated digital model of plate boundaries. *Geochemistry, Geo-*
 339 *physics, Geosystems*, *4*(3). doi: 10.1029/2001GC000252
- 340 Brune, J. N. (1971). Correction (to Brune, 1970). *J. geophys. Res.*, *76*, 5002.
- 341 Candela, T., Renard, F., Klinger, Y., Mair, K., Schmittbuhl, J., & Brodsky, E. E.
 342 (2012). Roughness of fault surfaces over nine decades of length scales. *Journal*
 343 *of Geophysical Research: Solid Earth*, *117*(B8). doi: 10.1029/2011JB009041
- 344 Cesca, S., Zhang, Y., Mouslopoulou, V., Wang, R., Saul, J., Savage, M., ... Dahm,
 345 T. (2017). Complex rupture process of the Mw 7.8, 2016, Kaikoura earth-
 346 quake, New Zealand, and its aftershock sequence. *Earth and Planetary Science*
 347 *Letters*, *478*, 110–120. doi: 10.1016/j.epsl.2017.08.024
- 348 Convers, J. A., & Newman, A. V. (2011). Global evaluation of large earthquake en-
 349 ergy from 1997 through mid-2010. *J. Geophys. Res. Solid Earth*. doi: 10.1029/
 350 2010JB007928
- 351 Danré, P., Yin, J., Lipovsky, B. P., & Denolle, M. A. (2019). Earthquakes Within
 352 Earthquakes: Patterns in Rupture Complexity. *Geophysical Research Letters*,
 353 *46*(13), 7352–7360. doi: 10.1029/2019GL083093
- 354 Denolle, M. A. (2019). Energetic Onset of Earthquakes. *Geophysical Research Let-*
 355 *ters*, *46*(5), 2458–2466. doi: 10.1029/2018GL080687
- 356 Denolle, M. A., & Shearer, P. M. (2016). New perspectives on self-similarity for
 357 shallow thrust earthquakes. *Journal of Geophysical Research: Solid Earth*,
 358 *121*(9), 2016JB013105. doi: 10.1002/2016JB013105
- 359 Dynamic Time Warping. (2007). In M. Müller (Ed.), *Information Retrieval for Mu-*
 360 *sic and Motion* (pp. 69–84). Berlin, Heidelberg: Springer. doi: 10.1007/978-3-
 361 -540-74048-3_4
- 362 Dziewonski, A. M., & Anderson, D. L. (1981). Preliminary reference Earth
 363 model. *Physics of the Earth and Planetary Interiors*, *25*(4), 297–356. doi:
 364 10.1016/0031-9201(81)90046-7
- 365 Eshelby, J. D. (1957). The determination of the elastic field of an ellipsoidal inclu-
 366 sion, and related problems. In *Proceedings of the Royal Society of London A:*
 367 *Mathematical, Physical and Engineering Sciences* (Vol. 241, pp. 376–396). The
 368 Royal Society.

- 369 Graves, R., & Pitarka, A. (2016). Kinematic Ground-Motion Simulations on Rough
370 Faults Including Effects of 3d Stochastic Velocity Perturbations Kinematic
371 Ground-Motion Simulations on Rough Faults. *Bulletin of the Seismological*
372 *Society of America*, *106*(5), 2136–2153. doi: 10.1785/0120160088
- 373 Guatteri, M., & Spudich, P. (2000). What Can Strong-Motion Data Tell Us about
374 Slip-Weakening Fault-Friction Laws? *Bulletin of the Seismological Society of*
375 *America*, *90*(1), 98–116. doi: 10.1785/0119990053
- 376 Houston, H. (2001). Influence of depth, focal mechanism, and tectonic setting
377 on the shape and duration of earthquake source time functions. *Journal of*
378 *Geophysical Research: Solid Earth*, *106*(B6), 11137–11150. doi:
379 10.1029/2000JB900468
- 380 Ide, S., & Beroza, G. C. (2001). Does apparent stress vary with earthquake size.
381 *Geophys. Res. Lett.*, *28*(17), 3349–3352.
- 382 Ide, S., & Takeo, M. (1997). Determination of constitutive relations of fault slip
383 based on seismic wave analysis. *Journal of Geophysical Research: Solid Earth*,
384 *102*(B12), 27379–27391. doi: 10.1029/97JB02675
- 385 Kanamori, H., Hong-Kie, T., Doug, D., Egill, H., & Heaton, T. (1992). Initial
386 investigation of the Landers, California, Earthquake of 28 June 1992 us-
387 ing TERRAscope. *Geophysical Research Letters*, *19*(22), 2267–2270. doi:
388 10.1029/92GL02320
- 389 Kaneko, Y., Fukuyama, E., & Hamling, I. J. (2017). Slip-weakening distance and
390 energy budget inferred from near-fault ground deformation during the 2016
391 Mw7.8 Kaikōura earthquake. *Geophysical Research Letters*, *44*(10), 4765–4773.
392 doi: 10.1002/2017GL073681
- 393 Kaneko, Y., & Lapusta, N. (2010). Supershear transition due to a free surface in
394 3-D simulations of spontaneous dynamic rupture on vertical strike-slip faults.
395 *Tectonophysics*, *493*(3), 272–284. doi: 10.1016/j.tecto.2010.06.015
- 396 Klinger, Y. (2010). Relation between continental strike-slip earthquake segmenta-
397 tion and thickness of the crust. *Journal of Geophysical Research: Solid Earth*,
398 *115*(B7). doi: 10.1029/2009JB006550
- 399 Li, Y.-G., Aki, K., Vidale, J. E., Lee, W. H. K., & Marone, C. J. (1994). Fine Struc-
400 ture of the Landers Fault Zone: Segmentation and the Rupture Process. *Sci-*
401 *ence*, *265*(5170), 367–370. doi: 10.1126/science.265.5170.367
- 402 Mai, P. M., & Beroza, G. C. (2002). A spatial random field model to characterize
403 complexity in earthquake slip. *Journal of Geophysical Research: Solid Earth*,
404 *107*(B11), ESE 10–1. doi: 10.1029/2001JB000588
- 405 Mai, P. M., Galis, M., Thingbaijam, K. K. S., Vyas, J. C., & Dunham, E. M.
406 (2017). Accounting for Fault Roughness in Pseudo-Dynamic Ground-
407 Motion Simulations. *Pure and Applied Geophysics*, *174*(9), 3419–3450. doi:
408 10.1007/s00024-017-1536-8
- 409 Massonnet, D., Rossi, M., Carmona, C., Adragna, F., Peltzer, G., Feigl, K., &
410 Rabaute, T. (1993). The displacement field of the Landers earthquake mapped
411 by radar interferometry. *Nature*, *364*(6433), 138–142. doi: 10.1038/364138a0
- 412 Meier, M.-A., Ampuero, J. P., & Heaton, T. H. (2017). The hidden simplicity of
413 subduction megathrust earthquakes. *Science*, *357*(6357), 1277–1281. doi: 10
414 .1126/science.aan5643
- 415 Meng, L., Ampuero, J.-P., Stock, J., Duputel, Z., Luo, Y., & Tsai, V. C. (2012).
416 Earthquake in a maze: Compressional rupture branching during the 2012 Mw
417 8.6 Sumatra earthquake. *Science*, *337*(6095), 724–726.
- 418 Peyrat, S., Olsen, K., & Madariaga, R. (2001, November). Dynamic modeling of
419 the 1992 Landers earthquake. *Journal of Geophysical Research: Solid Earth*,
420 *106*(B11), 26467–26482. doi: 10.1029/2001JB000205
- 421 Ripperger, J., Ampuero, J.-P., Mai, P. M., & Giardini, D. (2007). Earthquake
422 source characteristics from dynamic rupture with constrained stochastic
423 fault stress. *Journal of Geophysical Research: Solid Earth*, *112*(B4). doi:

- 424 10.1029/2006JB004515
 425 Shearer, P. M., Prieto, G. A., & Hauksson, E. (2006). Comprehensive analysis of
 426 earthquake source spectra in southern California. *Journal of Geophysical Re-*
 427 *search: Solid Earth*, *111*(B6). doi: 10.1029/2005JB003979
 428 Trugman, D. T., & Dunham, E. M. (2014). A 2d Pseudodynamic Rupture Model
 429 Generator for Earthquakes on Geometrically Complex Faults A 2d Pseudody-
 430 namic Rupture Model Generator for Earthquakes on Geometrically Complex
 431 Faults. *Bulletin of the Seismological Society of America*, *104*(1), 95–112. doi:
 432 10.1785/0120130138
 433 Vallée, M. (2013). Source time function properties indicate a strain drop indepen-
 434 dent of earthquake depth and magnitude. *Nature Communications*, *4*, 2606.
 435 doi: 10.1038/ncomms3606
 436 Vallée, M., Charléty, J., Ferreira, A. M. G., Delouis, B., & Vergoz, J. (2011).
 437 SCARDEC: a new technique for the rapid determination of seismic moment
 438 magnitude, focal mechanism and source time functions for large earthquakes
 439 using body-wave deconvolution. *Geophysical Journal International*, *184*(1),
 440 338–358. doi: 10.1111/j.1365-246X.2010.04836.x
 441 Vallée, M., & Douet, V. (2016). A new database of source time functions (STFs) ex-
 442 tracted from the SCARDEC method. *Physics of the Earth and Planetary Inte-*
 443 *riors*, *257*, 149–157. doi: 10.1016/j.pepi.2016.05.012
 444 Wessel, P., Smith, W. H. F., Scharroo, R., Luis, J., & Wobbe, F. (2013). Generic
 445 Mapping Tools: Improved Version Released. *Eos, Transactions American Geo-*
 446 *physical Union*, *94*(45), 409–410. doi: 10.1002/2013EO450001
 447 Wibberley, C. A. J., & Shimamoto, T. (2005). Earthquake slip weakening and asper-
 448 ities explained by thermal pressurization. *Nature*, *436*(7051), 689–692. doi: 10
 449 .1038/nature03901
 450 Yagi, Y., & Fukahata, Y. (2011). Rupture process of the 2011 Tohoku-oki earth-
 451 quake and absolute elastic strain release. *Geophysical Research Letters*, *38*(19).
 452 doi: 10.1029/2011GL048701

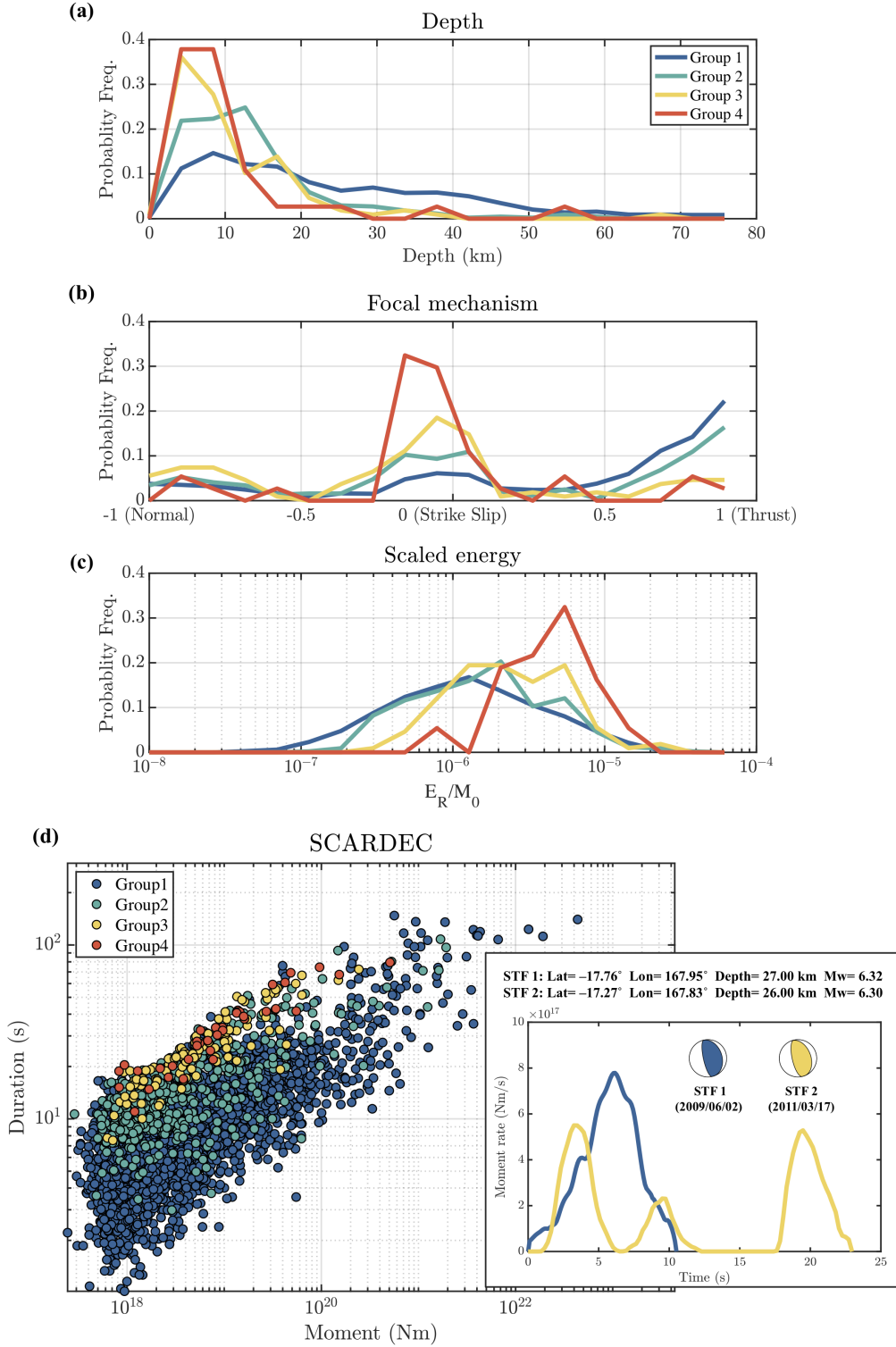


Figure 2. Population distribution of four complexity groups and correlation with different source parameters: (a) centroid depth, (b) focal mechanism (scalar defined by Shearer et al. (2006) that varies from -1 (normal), 0 (strike-slip) to 1 (reverse)), (c) and scaled radiated energy $e = E_R/M_0$. Panel (d) shows the earthquake duration against earthquake moment, colored with the respective group labels. One pair of co-located events with different complexity are also shown in the inset.

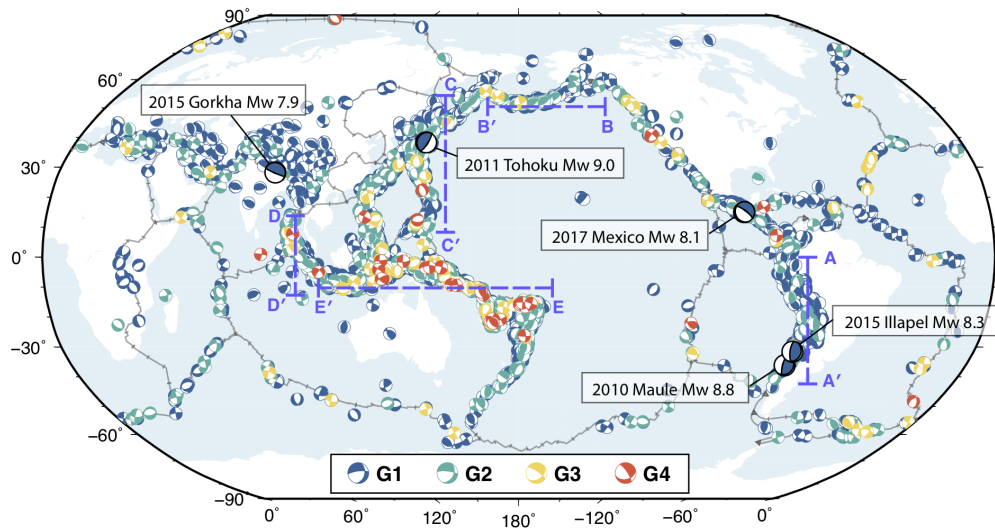


Figure 3. Map of focal mechanisms colored by their group label and overlay of the plate boundaries (gray thin lines). Several recent large megathrust earthquakes are highlighted. Blue dashed lines shown the locations of profiles in Figure 4. Bottom panels show the center STFs in each groups (same as those in Figure 1 (a)) as well as the corresponding schematic rupture propagation.

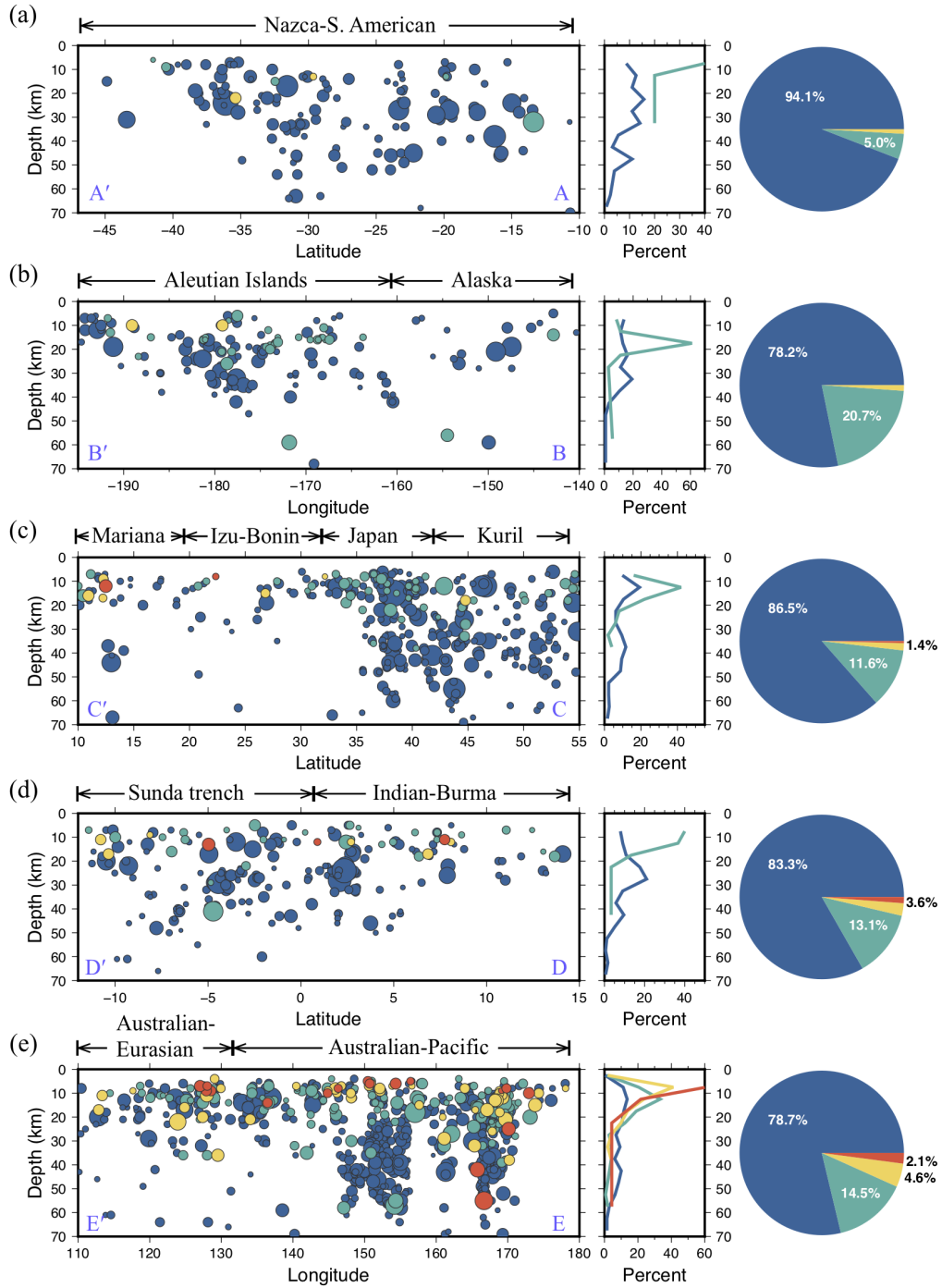


Figure 4. Earthquake distributions of different complexity groups on the vertical profiles (from 0–70 km, locations are indicated by blue dashed lines in Figure 3). The regional along-depth and total group distributions are also shown to the right.

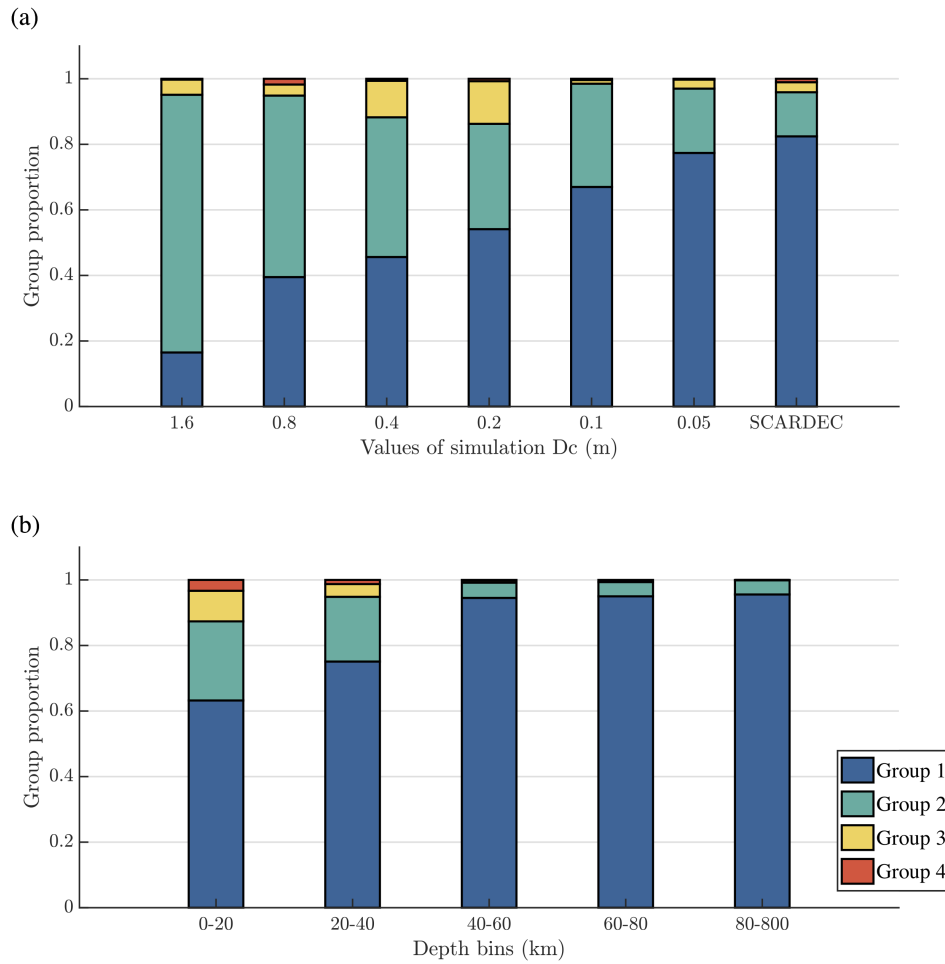


Figure 5. Group proportion distributions: (a) simulated STFs clustering with different values of D_c , compared with the group proportions of real STFs (SCARDEC); (b) Group proportions of real STFs (SCARDEC) within different depth bins.